THE JOURNAL OF PHYSICAL CHEMISTRY C

Article

pubs.acs.org/JPCC

Time-Resolved Infrared Vibrational Spectroscopy of the Photoinduced Phase Transition of $Pd(dmit)_2$ Salts Having Different Orders of Phase Transition

Naoto Fukazawa,[†] Takahiro Tanaka,[†] Tadahiko Ishikawa,[†] Yoichi Okimoto,[†] Shin-ya Koshihara,[†,‡] Takashi Yamamoto,[§] Masafumi Tamura,[∥] Reizo Kato,[⊥] and Ken Onda*[,#,¶]

[†]Department of Chemistry and Materials Science, Tokyo Institute of Technology, O-okayama, Meguro-ku, Tokyo 152-8551, Japan

[‡]CREST, Japan Science and Technology Agency (JST), O-okayama, Meguro-ku, Tokyo 152-8551, Japan

[§]Department of Chemistry, Graduate School of Science, Osaka University, Toyonaka, Osaka 560-0043, Japan

[∥]Department of Physics, Faculty of Science and Technology, Tokyo University of Science, Noda, Chiba 278-8510, Japan

[⊥]RIKEN, Wako, Saitama 351-0198, Japan

[#]Interactive Research Center of Science, Tokyo Institute of Technology, Nagatsuta, Midori-ku, Yokohama, Kanagawa 226-8502, Japan

[¶]PRESTO, Japan Science and Technology Agency (JST), 4-1-8 Honcho, Kawaguchi, Saitama 332-0012, Japan

ABSTRACT: To clarify the mechanism of the later process of photoinduced phase transition (PIPT) in organic charge-transfer complexes, we examined by time-resolved infrared vibrational spectroscopy two dimeric anion radical salts, $Et_2Me_2Sb[Pd(dmit)_2]_2$ (Et_2Me_2Sb salt) and $Cs[Pd(dmit)_2]_2$ (Cs salt) (Et, Me, and dmit are C_2H_5, CH_3, and 1,3-dithiol-2-thione-4,5-dithiolate, respectively), having similar characteristics except for the order of their phase transitions at thermal equilibrium. The phase transition is first order for the Et_2Me_2Sb salt and second order for the Cs salt at thermal equilibrium. Although both salts exhibit a high-temperature phase at later delay times (>100 ps) after the photoexcitation of the low-temperature phase, the time required for the emergence of the high-temperature phase was significantly different: 70 ps for the Et_2Me_2Sb salt and <0.1 ps for the Cs salt. The slow emergence of the high-temperature phase in the PIPT of the Et_2Me_2Sb salt presumably has an origin similar to that recognized for the first-order thermal phase transition, that is, steric effects of the Et_2Me_2Sb cation when the phase transitions occur.

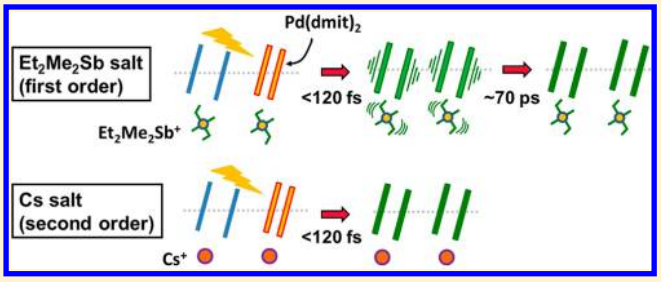

1. INTRODUCTION

Photoinduced phase transition (PIPT) is a cooperative phenomenon in which a few electrons injected by photoirradiation trigger a change in macroscopic physical properties through various interactions.[1−21] Since such phase transitions are ultrafast and efficient, they have attracted significant attention from the scientific viewpoint as well as for applications to ultrafast photoswitching devices. However, PIPT is very difficult to understand and utilize because it involves many nonequilibrium states including photoinduced phases from the Franck−Condon state to the thermal equilibrium state on the femtosecond to nanosecond time scales. Thus, various ultrafast techniques have been applied to address these difficulties. The first effort used conventional nanosecond and 100-fs lasers.[1,2] Sub-20-fs lasers have also been recently developed.[3−5] In terms of wavelength, it is now feasible to generate strong mid-infrared[6,7] to terahertz pulses,[8,9] and these have been applied to studies of PIPT. Time-resolved photoemission spectroscopy is also a powerful tool to study PIPT.[10]

These previous studies have successfully observed photoinduced changes in the electronic structure. Recently, methods to observe molecular and lattice structure, such as time-resolved diffraction[11−15] and time-resolved vibrational spectroscopy,[16−21] have been developed, and relatively slow structural dynamics in PIPT have attracted more attention. Time-resolved diffraction using ultrashort X-rays or electron-beams is a direct method, but requires large facilities and is still under development. On the other hand, time-resolved vibrational spectroscopy uses table-top lasers and is an established method for studying structural changes of molecules in the gas or liquid phases. Although conventional vibrational spectroscopy under steady-state conditions is popular for studying structure and charge in solid materials in thermal equilibrium, time-resolved vibrational spectroscopy is rarely used for studying photoinduced dynamics in solid materials. Thus, we have developed

Received: March 31, 2013
Revised: May 31, 2013
Published: June 4, 2013

dx.doi.org/10.1021/jp403193a | J. Phys. Chem. C 2013, 117, 13187−13196

time-resolved vibrational spectroscopy applicable to photo-induced dynamics in solid materials.[16−19]

Among the materials exhibiting PIPT, we have intensively studied organic charge transfer (CT) complexes.[22] CT complexes are single crystals consisting of small π-electron molecules and exhibit a wide variety of phases, such as metal, charge-ordered insulator, Mott insulator, and superconductor, by applying weak external stimuli, because they are essentially strongly correlated electron systems.[23−28] Moreover, CT complexes are suitable for applying time-resolved vibrational spectroscopy because their constituent molecules include the C═C stretching vibrational modes whose energies and intensities are sensitive to the structure and charge of the molecules.[31−40] We have found that approximately 100 ps are required for the emergence of the high-temperature phase in some types of CT complexes.[13,16,17,19] To elucidate the origin of this slow emergence of the high-temperature phase, it is useful to compare two samples that have the same characteristics except for one distinction. In this study, we considered two dimeric anion radical salts, $(C_2H_5)_2(CH_3)_2Sb[Pd(dmit)_2]_2$ (Et_2Me_2Sb salt) and $Cs[Pd(dmit)_2]_2$ (Cs salt) (dmit = 1,3-dithiol-2-thione-4,5-dithiolate), because they have almost the same crystal structures and charge distributions but the order of their thermal phase transition is different: the former is first order and the latter is second order. In first order phase transition, structural parameters jump at phase transition temperature accompanied by latent heat, whereas in second order phase transition, they vary smoothly; thus, information on dynamical structure change is expected to be obtained.

The CT complexes consisting of a $Pd(dmit)_2$ anion, $Z[Pd(dmit)_2]_2$ (Z is a monovalent cation), show diverse phases such as metal (M), dimer Mott insulator (DM), charge separation (CS), valence bond liquid, and valence bond solid because of the competition and frustration of interactions among charges and spins in the two-dimensional triangular lattice.[27,28,41−47] A phase diagram based on the structures and resistivity measurements has been proposed for β'-$Z[Pd(dmit)_2]_2$.[27,28] The compounds in this series are on the boundary of Mott transitions, suggesting that they are strongly charge correlated systems. Moreover, they have layered crystal structures, in which conducting anion layers consisting of $Pd(dmit)_2$ and insulating cation layers consisting of Z are alternately stacked. In the anion layer, $[Pd(dmit)_2]_2^-$ dimers are stacked face-to-face in different directions from layer to layer (along the $a + b$ and $a - b$ axis) forming a solid-crossing column structure in most cases. There is tight dimerization of the $Pd(dmit)_2$ molecules; thus, the dimer has been thought to be an effective unit and constitutes a half-filled band system.

Among these salts, only the Et_2Me_2Sb and Cs salts exhibit a unique complete charge-separated (CS) phase. The formal charge of the $Pd(dmit)_2$ molecule in these salts is −0.5, and the system has a half-filled character owing to the tight dimerization.[47−49] As shown in Figure 1a, at room temperature, the charge on each $[Pd(dmit)_2]_2$ dimer is uniformly −1 (monovalent) in both the salts, and the phases of the Et_2Me_2Sb and Cs salts are dimer Mott insulator (DM) and metal (M), respectively. At low temperatures, both salts undergo a phase transition to the same CS phase in which the dimer charges of −2 (divalent) and 0 (neutral) are ordered at about 70 K for the Et_2Me_2Sb and 60 K for the Cs salts.[44] X-ray structural analysis has revealed that these salts show the same structural changes (space groups and lattice and dimer structures) at the phase transition.[44] In contrast, the order of phase transition for these

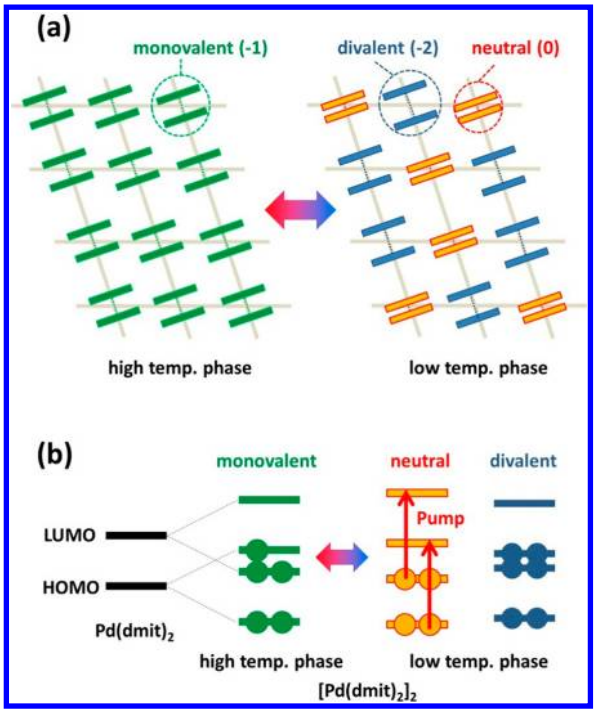

Figure 1. (a) Common charge patterns and crystal structures in the high- and low-temperature phases of $(C_2H_5)_2(CH_3)_2Sb[Pd(dmit)_2]_2$ (Et_2Me_2Sb salt) and $Cs[Pd(dmit)_2]_2$ (Cs salt). (b) Stabilization of the low-temperature phase when $Pd(dmit)_2$ forms a tight dimer. The red arrows indicate the transition induced by the pump pulse (800 nm, 1.55 eV).

salts is significantly different. The lattice parameters of the Et_2Me_2Sb salt are discontinuously changed at the transition temperature, whereas those of the Cs salt are continuously changed. Moreover, their transport and magnetic properties vary similarly with their lattice parameters.[47,50,51] Thus, the phase transition is considered to be first order for the Et_2Me_2Sb salt and second order for the Cs salt.[44] As described in detail later, this difference in order of phase transition originates from the shape of the cations. The hook-shaped Et_2Me_2Sb cation works like a latch in the phase transition whereas the spherical Cs cation does not exhibit such an effect.[44]

The thermal phase transition in these salts is governed by the stability of their molecular orbitals. Figure 1b shows the schematic energy levels of the molecular orbitals of the $Pd(dmit)_2$ salts. When they form a dimer, $[Pd(dmit)_2]_2$, each HOMO and LUMO level of the $Pd(dmit)_2$ molecules is split into two levels, associated with bonding and antibonding pairs.[52] If the molecules form a tight dimer, that is, the overlap between the molecules is large, the energy levels of the antibonding pair of HOMOs and the bonding pair of LUMOs are exchanged. Both the two bonding levels become located in the lower energy region owing to this energy-level exchange, so that the neutral dimer is strongly stabilized. Because the energy gain by this neutral dimer formation is greater than the energy loss by the divalent dimer formation, the CS phase is preferred at low temperatures.[27,44,48−50] Accompanying this stabilization, the intradimer distance between the $Pd(dmit)_2$ molecular planes is characteristically changed, as shown in Figure 1a. The distance between the planes in the neutral dimer decreases and a tighter dimer is formed (indicated in orange); alternatively, that between the planes in the divalent dimer increases and the looser dimer is formed (indicated in blue).

dx.doi.org/10.1021/jp403193a | J. Phys. Chem. C 2013, 117, 13187−13196

Previously, we studied PIPT triggered by the destabilization of the neutral or divalent dimer by photoirradiation.[51] For the Et_2Me_2Sb salt, time-resolved reflectivity-change measurements in the near-infrared region showed that the charge of the dimers becomes uniformly monovalent within 120 fs by the photoexcitation of the low-temperature CS phase. In the Cs salt, a similar result was obtained.[53] However, we only observed changes in the electronic states of the dimer, which reflects the distance between the two molecules in the dimer. Thus, in the current study we investigated the hidden PIPT dynamics by the previous near-infrared spectroscopy method using time-resolved infrared vibrational spectroscopy in terms of variations in the structure and charge of the constituent molecules.

2. EXPERIMENTAL METHODS

The experimental setup for time-resolved infrared vibrational spectroscopy has been reported previously[16] and thus it is described in brief here. Time-resolved vibrational spectra were measured using a broadband femtosecond mid-infrared pulse and a linear infrared detector array. The broadband mid-infrared probe pulse (pulse duration, 120 fs; tunable range, 1000−3700 cm^{-1}; spectral width, 150 cm^{-1}) was generated by optical parametric amplification (OPA) and difference frequency generation (DFG) from the output of a femtosecond Ti:sapphire regenerative amplifier operating at 1 kHz (center wavelength, 800 nm). The near-infrared pump pulse (800 nm) was obtained from a part of the output of a Ti:sapphire amplifier. The spot size of the probe pulse (0.1 mmϕ) was much smaller than that of the pump pulse (0.4 mmϕ) at the sample surface in order to avoid inhomogeneous excitation. The probe pulse reflected from the sample was detected by a 64-channel linear MCT (HgCdTe) array through a 19-cm polychromator. The energy resolution of this system was approximately 3 cm^{-1}. The pulse train of the pump pulse was modulated at 500 Hz with an optical chopper to obtain data with a higher signal-to-noise ratio. The delay time between the pump and probe pulses was obtained by an optical delay line and the maximum delay time was 1 ns. The sample crystals were made by an oxidation process of $[Et_2Me_2Sb]_2[Pd(dmit)_2]_2$.[54] The typical crystal size was approximately 1.0 × 0.5 × 0.2 mm^3. Linear reflectivity spectra without a pump pulse were measured using a Fourier transform infrared (FTIR) spectrometer equipped with a Cassegrain microscope objective lens. The crystal was held inside a conduction-type cryostat and was maintained at 50 K for the Et_2Me_2Sb salt and 20 K for the Cs salt during pump−probe measurements.

3. RESULTS AND DISCUSSION

3.1. Et_2Me_2Sb Salt. In dimeric $Pd(dmit)_2$ salts, the C═C stretching vibrational bands are located between 1250 and 1400 cm^{-1}.[39] Figure 2 shows the vibrational modes originating from the dimerization of $Pd(dmit)_2$. In a $Pd(dmit)_2$ monomer, the two C═C bonds shown in Figure 2a contribute two stretching vibrational modes: a ν_1 Raman-active mode and a ν_2 infrared-active mode, because the monomer has an inversion symmetry, as shown by the arrows in Figure 2b. When the monomers form a tight dimer, $[Pd(dmit)_2]_2$, four vibrational modes emerge by a combination of the four C═C bonds, as shown in Figure 2c. The B and C modes are IR active, whereas the A and D modes are Raman active, also because the center of the inversion symmetry lies at the center of the dimer. Of these four modes, the B mode is insensitive to the structure of the

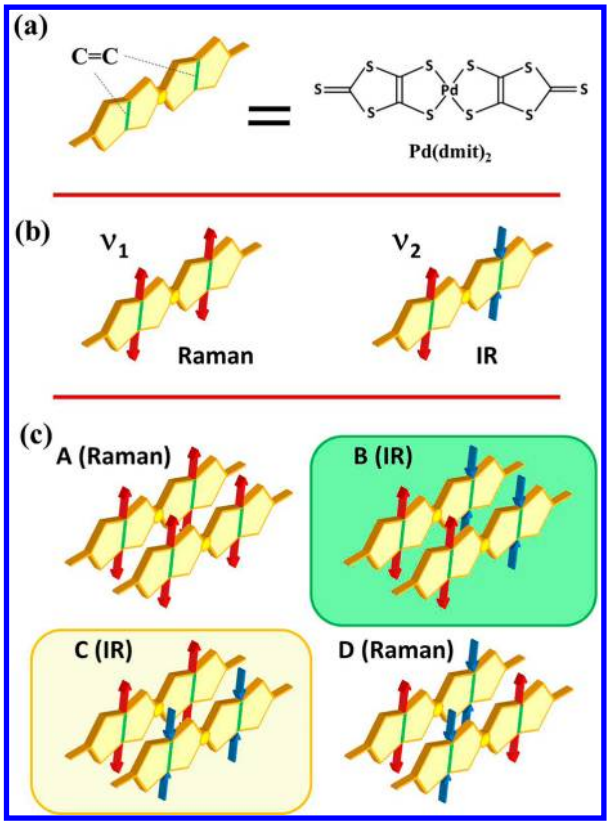

Figure 2. Vibrational modes induced by the dimerization of $Pd(dmit)_2$. (a) C═C bonds contributing to the vibrational modes. (b) Two vibrational modes of the $Pd(dmit)_2$ monomer including the variation of the C═C bonds. (c) Four vibrational modes induced by forming the tight dimer $[Pd(dmit)_2]_2$.

dimer and its center frequency is sensitive to the charge of a monomer because the main contribution to the B mode is the infrared-active monomer mode ν_2, whereas the Raman active A mode is not sensitive to the charge at a monomer but to the charge of the dimer.[55] The frequency difference between the neutral and divalent dimers is 50−80 cm^{-1}.[39] In contrast, the frequency and intensity of the C mode strongly depend on both the intra- and interdimer overlap integrals whereas those of the D mode depend mostly on the intradimer overlap integral; thus, the C mode is a good probe for both the intradimer structure (the relative position of the molecules inside a dimer) and interdimer structure (the relative position between dimers), and the D mode is a good probe for the intradimer structure.[39]

Figure 3a shows the linear reflectivity spectra of the Et_2Me_2Sb salt in the low-temperature phase at 50 K (blue line) and in the high-temperature phase at 300 K (red line). These were measured using linearly polarized light parallel to the *a*-axis (E||a). In the low-temperature phase, the C mode (C_{LT}) emerges as a broad band spanning 1250−1310 cm^{-1}. This broad bandwidth is caused by the interdimer interactions.[56] This band has two dips at approximately 1263 and 1302 cm^{-1} due to anti-resonance of the D mode (D_{LT}).[39,57] In the high-temperature phase, there are two obvious bands: the one at approximately 1330 cm^{-1} is assigned to the B mode (B_{HT}) and the other at approximately 1290 cm^{-1} is assigned to the C mode (C_{HT}).[39] Note that the spectral patterns are drastically changed from the low- to high-temperature phases reflecting the difference in charge and structure of their phases.

dx.doi.org/10.1021/jp403193a | J. Phys. Chem. C 2013, 117, 13187−13196

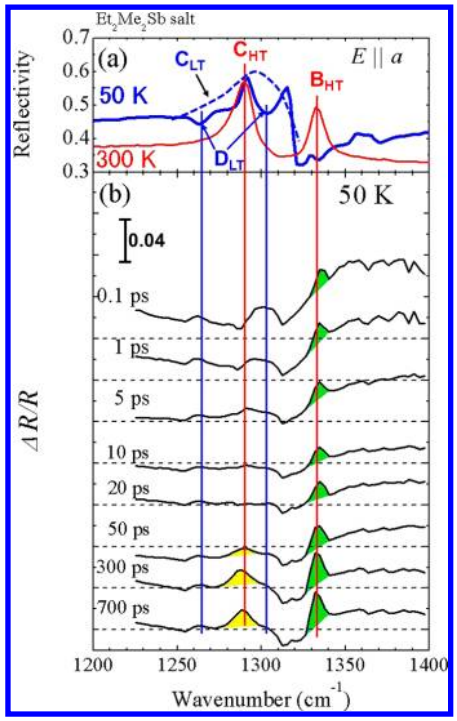

Figure 3. (a) Polarized linear reflectivity spectra of the Et_2Me_2Sb salt in the low-temperature phase at 50 K (blue line) and in the high-temperature phase at 300 K (red line). The polarization of light (E) is parallel to the *a*-axis of the crystal (E||a). The dashed line represents the C mode band (C_{LT}) without anti-resonance of the D mode band (D_{LT}) in the low-temperature phase as a guide for the eyes. B_{HT} and C_{HT} represent the B and C mode bands in the high-temperature phase, respectively. (b) Selected transient vibrational reflectivity change ($\Delta R/R$) spectra obtained with a E||a probe pulse of 0.1−700 ps by photoexcitation at 800 nm in the low-temperature phase at 50 K. The green and yellow areas represent the B_{HT} and C_{HT} bands induced by photoexcitation, respectively. The dashed horizontal lines represent the zero level for each spectrum.

Figure 3b shows the transient vibrational spectra observed at 0.1, 1, 5, 10, 20, 50, 300, and 700 ps after the photoexcitation of the low-temperature CS phase at 50 K. The vertical axis represents the reflectivity change ($\Delta R/R$). The wavelength and intensity of the pump pulse were 800 nm (1.55 eV) and 0.27 mJ/cm^2 (1.1×10^{15} photons/cm^2), respectively, and the polarizations of the pump and probe pulses were parallel to the *a*-axis (E||a). The photon energy corresponds to the electronic transition from the bonding to the antibonding orbital in the neutral dimer, as shown by the red arrows in Figure 1b. This photoexcitation destabilizes the dimerization of the neutral dimer. At 0.1 ps, a reflectivity increase over a wide spectral region spanning 1225−1400 cm^{-1} was observed. This wide-range spectral change is mainly attributed to the change in the interdimer CT absorption band. In addition to the wide-range spectral change, there are at least two relatively sharp bands (marked in green and yellow in Figure 3b). The green band emerges immediately after photoexcitation, and its spectral strength increases gradually over 300 ps. In contrast, the yellow band emerges only after 50 ps. Based on their wavenumbers, the green and yellow bands are assigned to the B_{HT} and C_{HT} bands in the high-temperature phase, respectively. In addition, there are relatively small bands at the positions of the anti-resonance dips of the D_{LT} mode indicated by the blue lines from the beginning of the delay time.

To confirm these assignments, we performed a spectral simulation using the multilayer model typically used for the analysis of photoinduced phase transitions.[19,58−61] In this simulation, we assumed that the dielectric constant before and after photoexcitation correspond to the dielectric constants, which are deduced from the reflectivity spectra using the Kramers−Kronig transformation, of the low- and high-temperature phases, respectively, and that the density of the photoinduced phase decreases exponentially with penetration depth, *d*, along the direction of the propagation of the pump light from the sample surface. The sample is represented as a model composed of many thin layers having the same thickness and different but homogeneous dielectric constants. The dielectric constant of each layer is assumed from the following formula

$$\varepsilon(x) = \varepsilon^{HT}\gamma \exp\left(-\frac{x}{d}\right) + \varepsilon^{LT}\left\{1 - \gamma \exp\left(-\frac{x}{d}\right)\right\}$$

In this formula, the dielectric constant is represented by a linear combination of the dielectric constants of the low- (ε^{LT}) and high-temperature (ε^{HT}) phases considering the distribution of each phase, which is a function of the depth (x) from the sample surface. γ represents the ratio of the photoinduced phase at the sample surface. Under these assumptions, the photoinduced reflectivity spectrum is calculated from the transfer matrix by considering the contributions of each layer (for details of the calculation, see refs 19, 58). The spectrum simulated by this model is indicated by the red line in Figure 4

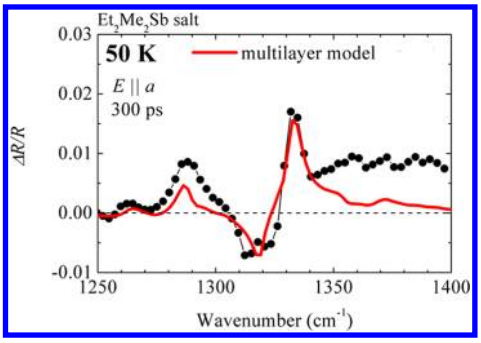

Figure 4. Transient vibrational reflectivity spectrum of the Et_2Me_2Sb salt at 300 ps (E||a) (black dots and line) and the simulated spectrum using the multilayer model (for details, see the text).

and is shown together with the spectrum at 300 ps (black dots and line). In the simulation, the value of 0.1 for the parameter γ and the value of 50 nm for the parameter *d* are estimated from the absorption coefficient at 800 nm in the low-temperature phase. We used the dielectric constants derived from the linear spectra in the low and high temperature phases for the values of $\varepsilon^{LT}$and ε^{HT}, respectively. The simulated spectral shape is in good agreement with that at 300 ps, except for some deviation above 1345 cm^{-1}, presumably due to the effect of the domain walls, which is not considered in our simulation. Thus, we concluded that the photoinduced phase at least after 300 ps is the same as the high-temperature phase, and the green and yellow bands are assigned to the B_{HT} and C_{HT} bands, respectively. On the other hand, the spectrum before 50 ps cannot be reproduced by our calculation owing to the absence of the C_{HT} band, strongly indicating the existence of a transient state.

dx.doi.org/10.1021/jp403193a | J. Phys. Chem. C 2013, 117, 13187−13196

As mentioned above, the B band is sensitive to the charge of the dimer whereas the C band is sensitive to the dimer structure; thus, the emergence of the B_{HT} and C_{HT} bands following photoexcitation indicates that the charge and the structure of the dimer become similar to those observed in the high-temperature phase. The empirical finding that the B_{HT} band emerges immediately after photoexcitation indicates that the divalent and neutral charges of the dimer in the low-temperature phase become averaged into a monovalent charge immediately after photoexcitation. In contrast, the fact that the C_{HT} emerges only after 50 ps indicates that it takes several tens of picoseconds for the structure of the dimer to resemble that observed in the high-temperature phase. We compare these temporal variations to the previous time-resolved study in the near-infrared region under the same condition, which observes different aspect of the same dynamics.[51] Based on the previous study, the structure of the intradimer becomes equivalent to that in the high-temperature phase within the pulse duration of approximately 120 fs. Considering that the C band is sensitive to both the intra- and interdimer structure, the slow dynamics must originate from the fluctuation of the interdimer structure.

Despite the relatively minor change, the disappearance of the dips of the D_{LT} mode contains important information about the early dynamics of the transient state. As pointed out above, there are small bands at the positions of the anti-resonance dips of the D_{LT} mode from the beginning of the delay time. It is reasonable that the emergence of these bands originates from the disappearance of the D_{LT} mode. Because the D mode is sensitive only to the intradimer structure, the emergence of these small bands indicates that the intradimer structure is changed from that in the low temperature phase immediately after photoexcitation. This result is also consistent with the previous time-resolved study in the near-infrared region.[51] Note that the fact that the D_{LT} bands appear to decrease at around 20 ps is presumably attributed to the variation and fluctuation of the background because the state is far from stable in this time region.

To confirm these results, we also measured the transient vibrational spectra of the same sample using a probe pulse polarized along a different crystal axis. Figure 5a shows the linear reflectivity spectra of the Et_2Me_2Sb salt in the low-temperature phase at 50 K (blue line) and in the high-temperature phase at 300 K (red line) measured using a linearly polarized light parallel to the *b* axis (E||b). According to ref 39, the bands at approximately 1290 cm^{-1} (C_{HT}) and 1335 cm^{-1} (B_{HT}) in the high-temperature phase were assigned to the B and C modes, respectively. The dips (D_{LT}) originating from the anti-resonance of the D mode in the C mode band (C_{LT}) are also observed at approximately 1270 and 1285 cm^{-1} in the low-temperature phase.

The transient vibrational spectra were measured at 0.1−400 ps after the photoexcitation of the low-temperature phase at 50 K using probe light polarized parallel to the *b*-axis of the crystal. The excitation intensity of the pump pulse polarized parallel to the *a*-axis was 1.1 mJ/cm^2 (4.5×10^{15} photons/cm^2). Selected transient $\Delta R/R$ spectra are shown in Figure 5b including the correlation between spectral changes and the delay time. Similar to the result using the E||a probe, at 0.1 ps, the reflectivity increases over the entire wavenumber range of the observed spectrum. The B_{HT} band (marked in green) emerges immediately after photoexcitation, and its intensity gradually increases up to 100 ps, whereas the C_{HT} band (marked in yellow) clearly emerges after 50 ps although there is a tiny band

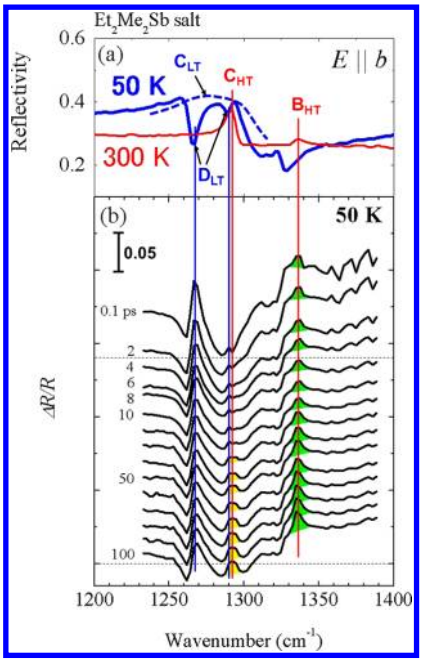

Figure 5. (a) Polarized linear reflectivity spectra of the Et_2Me_2Sb salt in the low-temperature phase at 50 K (blue line) and in the high-temperature phase at 300 K (red line). The polarization of light (E) is parallel to the *b* axis of the crystal (E||b). The dashed line represents the C mode band (C_{LT}) without anti-resonance of the D mode band (D_{LT}) in the low-temperature phase. B_{HT} and C_{HT} represent the locations of the B and C mode bands in the high-temperature phase, respectively. (b) Selected vibrational reflectivity change ($\Delta R/R$) spectra obtained with a E||b probe pulse of 0.1−100 ps by photoexcitation at 800 nm in the low-temperature phase at 50 K. The green and yellow areas represent the B_{HT} and C_{TH} bands in the transient spectra induced by photoexcitation, respectively. The dashed horizontal line represents the zero level for the spectrum at 0.1 and 100 ps.

before 50 ps. Furthermore, a simulated spectrum with different γ(=0.6), corresponding to the difference in excitation intensity shows good correlation with the transient spectrum at 300 ps, as shown by the red line in Figure 6. All these results are in good agreement with the results of the E||a probe.

The spectral change at the anti-resonance dips of the D_{LT} mode is also suggestive. The large and tiny bands emerge at the positions of the dips (approximately 1270 and 1285 cm^{-1}) from the beginning of the delay time. Considering that the D mode is sensitive to the intradimer structure, this indicates a

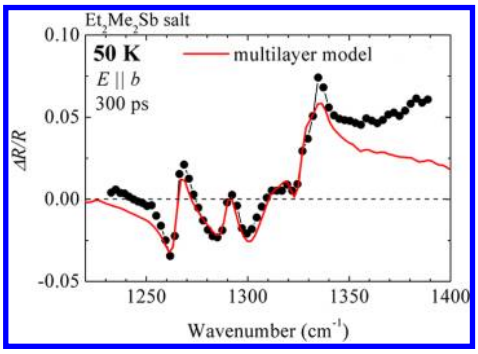

Figure 6. Transient vibrational reflectivity spectrum of the Et_2Me_2Sb salt at 300 ps (E||b) (black dots and line) and the simulated spectrum using the multilayer model (for details, see the text).

dx.doi.org/10.1021/jp403193a | J. Phys. Chem. C 2013, 117, 13187−13196

disappearance of the intradimer structure in the low-temperature phase immediately after photoexcitation. This result is also in good agreement with the results of the time-resolved study in the near-infrared region as well as those of the E||a probe. Thus, we concluded that the divalent and neutral charges of the dimers converge to monovalent charges and also the intradimer structure becomes similar to that in the high-temperature phase immediately after photoexcitation, whereas it takes tens of picoseconds for the interdimer structure to be converted into a structure similar to that in the high-temperature phase.

To obtain the temporal behavior of the B_{HT} and C_{HT} bands, the areas of these bands (indicated by colors in the figures) are plotted as a function of the delay time in Figure 7. Figures 7a and b show the temporal profiles of the B_{HT} and C_{HT} bands, respectively; the black dots and blue circles in both figures represent the normalized area obtained from the spectra of E||b and E||a, respectively. Although the quality of the data points of E||a diminishes owing to experimental issues, the temporal profiles of E||b and E||a are the same. The area of the B_{HT} band rapidly increases after photoexcitation followed by more gradual increases, whereas the area of the C_{HT} band gradually increases from the beginning of the observation period. The time constants of the consistently gradual increase were determined by a least-squares fit using the following equation:

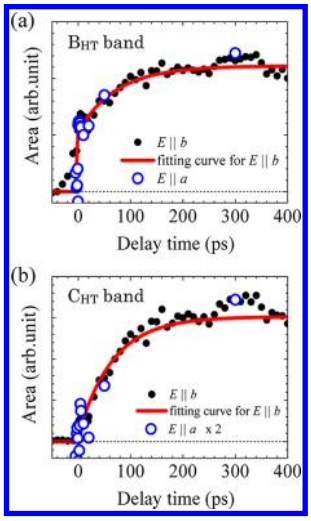

Figure 7. Temporal profiles of the area of the B_{HT} band (a) and the C_{HT} band (b) in the transient reflectivity change spectra of the Et_2Me_2Sb salt. The black dots and blue circles represent the data obtained with a E||b and E||a probe pulses, respectively. The red line is the fitting curve using eq 1 with a time constant of 70 ± 9 ps for the B_{HT} band and 66 ± 5 ps for the C_{HT} band.

$$f(t) = \begin{cases} 0 & (t < 0) \\ A\left\{1 - \exp\left(-\frac{t}{\tau}\right)\right\} + C & (t \geq 0) \end{cases} \quad (1)$$

where A is the magnitude of the component and τ is the time constant. In addition, by considering the instrumental function of the measurement system, the fitting function 1 was convoluted with a Gaussian function. The simulated curves shown by the red lines in Figures 7a and b adequately reproduce the temporal profiles of the area of the B_{HT} and C_{HT} bands, respectively. The time constants of the B_{HT} and C_{HT} bands are determined to be 70 ± 9 ps and 66 ± 5 ps, respectively, and are regarded as essentially equivalent within experimental error. From this analysis, it is concluded that the charge distribution evolves to the approximate charge distribution observed in the high-temperature phase within the pulse duration (~120 fs), and subsequently, the lattice structure transforms at above approximately 70 ps into one resembling that in the high-temperature phase. The difference in the charge distribution between immediately after photoexcitation and at later delay times (>100 ps) presumably originates from structural fluctuations that occur until the structure is stabilized.

3.2. Cs Salt. To compare the PIPT dynamics to those of a complex undergoing a second-order phase transition, we measured and analyzed the transient vibrational spectra of the Cs salt in a manner similar to that used for the Et_2Me_2Sb salt. Figure 8a shows the linear reflectivity spectra at 1200−1400 cm^{-1} measured using linearly polarized light parallel to the a axis at 20 K (low-temperature phase) and 100 K (high-temperature phase). Although the exact wavenumbers of the B and C bands have not yet been clarified, the bands corresponding to the B and C bands are located in this wavenumber region, as expected, because the Cs and Et_2Me_2Sb salts have similar crystal structures.

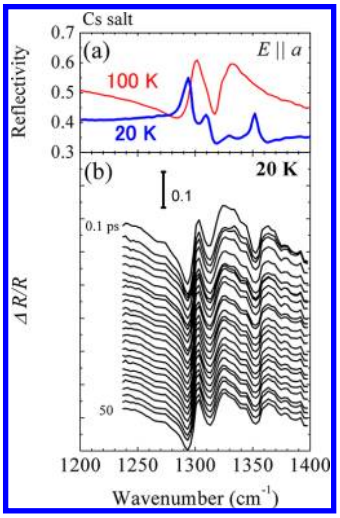

Figure 8. (a) Polarized linear reflectivity spectra of the Cs salt in the low-temperature phase at 20 K (blue line) and in the high-temperature phase at 100 K (red line). The polarization of light (E) is parallel to the a axis of the crystal (E||a). (b) Selected vibrational reflectivity change $\Delta R/R$) spectra obtained at 0.1−50 ps by photoexcitation at 800 nm in the low-temperature phase at 20 K.

Transient vibrational spectra were also measured at 0.1−50 ps after the photoexcitation of the low-temperature phase at 20 K. The probe pulse was polarized parallel to the a-axis of the crystal. The excitation intensity of the pump pulse at 800 nm was 0.44 mJ/cm^2 (1.8×10^{15} photons/cm^2), and the polarization of the pump pulse was also parallel to the a axis. Selected transient $\Delta R/R$ spectra are shown in Figure 8b. In striking contrast to the results of the Et_2Me_2Sb salt, the spectral changes of the Cs salt were consistent over the measured temporal range. As shown in Figure 9, the spectra were also well reproduced by the multilayer model with γ = 1.0. This value implies that one photon makes about two photo-converted dimers. Thus, it is concluded that a phase having a

dx.doi.org/10.1021/jp403193a | J. Phys. Chem. C 2013, 117, 13187−13196

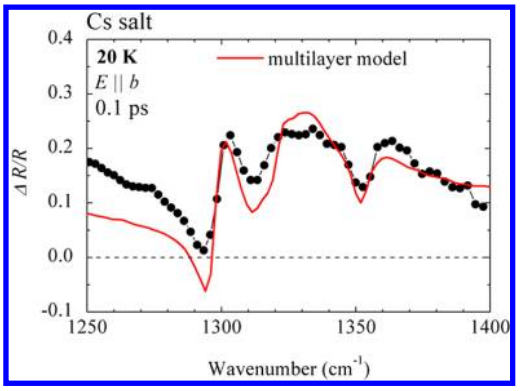

Figure 9. Selected transient vibrational reflectivity spectrum of the Cs salt at 300 ps (E||a) (black dots and line) and the simulated spectrum using the multilayer model (for details, see the text).

charge and structure similar to those in the high-temperature phase emerges immediately after photoexcitation, and the emerged phase persists for more than 50 ps. The details of the early dynamics of the Cs salt studied in terms of transient electronic spectra employing time-resolved near-infrared spectroscopy will be published elsewhere.[53]

3.3. Photoinduced Phase Transition Vs Thermal Phase Transition. Through the photoexcitation of the low-temperature CS phase in the Et_2Me_2Sb and Cs salts, it is found that the high-temperature phase emerges after at least 100 ps for both salts, but their temporal behaviors prior to the emergence of the high-temperature phase are different. For the Et_2Me_2Sb salt, the charge and intradimer structure become similar to those in the high-temperature phase immediately after photoexcitation, and subsequently the structure of the interdimer approaches that in the high-temperature phase over approximately 70 ps. In the Cs salt, the charge and all structures of the dimer transform into those in the high-temperature phase immediately after photoexcitation. At thermal equilibrium, the two salts have the same crystal structure both above and below the transition temperature, but their orders of phase transition are different; that is, the phase transition is first order for the Et_2Me_2Sb salt and second order for the Cs salt. This situation is clearly seen in the temperature dependence of the lattice parameters in the previous report.[44] Both temperature dependences resemble each other except for the jumps at the critical temperature for the Et_2Me_2Sb salt. Thus, the remaining major difference between the two salts is the structure of their cations. The Et_2Me_2Sb cation has four alkyl groups that resemble a hook, whereas the Cs cation is spherical. Thus, this difference in the cation structure, rather than the difference in electronic states (insulating or metallic), must be the cause of the difference in the temporal behavior of the PIPT and the order of the thermal phase transitions.[41] In X-ray crystal structure analysis,[44] it was found that there is a steric interaction between the alkyl groups of the Et_2Me_2Sb cation and the terminal S atoms of the $Pd(dmit)_2$ molecule accompanying the thermal phase transition. This steric effect requires latent heat at the thermal phase transition and causes the first-order phase transition. In contrast, the spherical Cs cation exhibits no steric effect, and the Cs salt undergoes a second-order phase transition. This steric effect must be responsible for the slow change of the interdimer structure during PIPT in the Et_2Me_2Sb salt. Immediately after CT excitation in the dimer by the excitation pulse, the charge and internal structure of the dimer transform to resemble those observed in the high-temperature phase. Afterward, the steric effect creates a bottleneck in the process of stabilization of the interdimer structure. On the other hand, the high-temperature phase emerges immediately after photoexcitation in the Cs salt because there is no steric interaction. In addition, it is also possible that the stronger interaction between the anion layers due to the small spherical Cs cation promotes the emergence of the high-temperature phase. Figure 10 illustrates the differences between the Et_2Me_2Sb and Cs salts for the PIPT process.

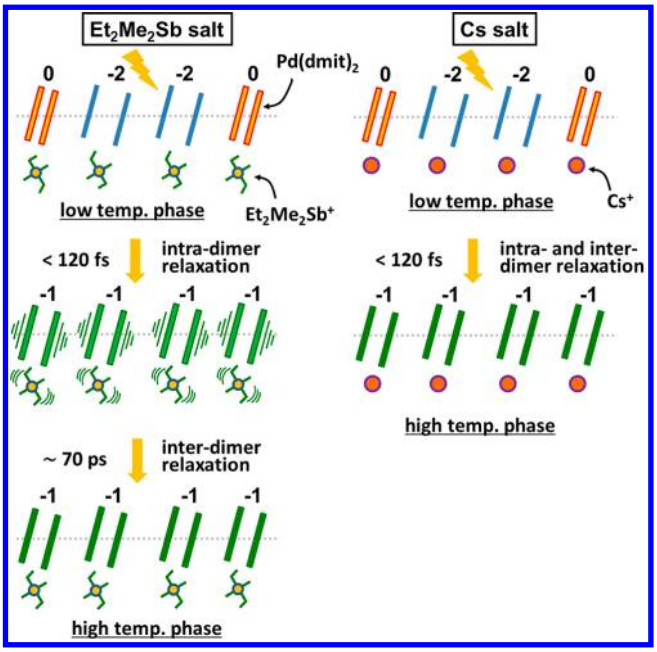

Figure 10. Differences between the Et_2Me_2Sb and Cs salts for the photoinduced phase transition process. Steric effects of the Et_2Me_2Sb cation cause a bottleneck in the course of the stabilization of the whole structure. The number above each dimer represents the charge on the dimer.

A similar situation was observed for the PIPT in $(EDO\text{-}TTF)_2PF_6$ (EDO-TTF: ethylenedioxy-tetrathiafulvalene).[19] After the peculiar photoinduced phase emerges, it takes approximately 100 ps for the charge and structure of EDO-TTF to become similar to those in the high-temperature phase. According to a recent study using time-resolved electron diffraction,[13] during this slow process, flat EDO-TTF molecules, which have less steric effect, move quickly less than 1 ps, whereas bent EDO-TTF molecules, which have more steric effect, vary slowly over 100 ps. Intriguingly, these time scales are consistent with our results. Although the situation is slightly different, a similarly slow process (~100 ps) was observed in the PIPT from the low- to high- temperature phase in TTF-CA (tetrathiafulvalene-*p*-chloranil).[17,62] In this slow process, proliferation of the domain occurs; however, this crystal also undergoes a first-order thermal phase transition, and there is probably a bottleneck slowing the proliferation process.

4. SUMMARY

We have examined the photoinduced phase transition mechanism by comparing two charge-transfer complexes having thermal phase transitions of different order by time-resolved infrared vibrational spectroscopy. For this purpose, we considered two dimeric anion radical salts, $(C_2H_5)_2(CH_3)_2Sb[Pd(dmit)_2]_2$ (Et_2Me_2Sb salt) and $Cs[Pd(dmit)_2]_2$ (Cs salt)

dx.doi.org/10.1021/jp403193a | J. Phys. Chem. C 2013, 117, 13187−13196

(dmit = 1,3-dithiol-2-thione-4,5-dithiolate), having the same crystal structure and charge distribution but exhibiting first- and second-order phase transitions, respectively. We monitored the vibrational bands that are sensitive to the charge or structure of the dimer, $[Pd(dmit)_2]_2$, as a function of the delay time. For the Et_2Me_2Sb salt, we observed that the charge distribution and intradimer structure are transformed into those similar to the high-temperature phase immediately after photoexcitation, and that it takes approximately 70 ps for the interdimer structure to resemble that observed in the high-temperature phase. For the Cs salt, we observed that the charge and intra- and interdimer structures are transformed into those in the high-temperature phase immediately after photoexcitation. The reason for the slow interdimer structural change is believed to originate from the steric effects of the Et_2Me_2Sb cation, which is also the origin of the first-order thermal phase transition in the Et_2Me_2Sb salt. This conclusion is a plausible explanation for the other results that show a slow emergence of the high-temperature phase with a time constant of approximately 100 ps in $(EDO\text{-}TTF)_2PF_6$ and TTF-CA by time-resolved infrared vibrational spectroscopy. Thus, it is possible that this concept is generally applicable to understanding photoinduced phase transitions in organic crystals.

AUTHOR INFORMATION

Corresponding Author

*Phone/fax: +81- 45-924-5891. E-mail: onda.k.aa@m.titech.ac.jp.

Notes

The authors declare no competing financial interest.

ACKNOWLEDGMENTS

This study was partly supported by a Grant-in-Aid for Scientific Research (B) (No. 20340074), a Grant-in-Aid for Scientific Research on Innovative Areas (No. 21110512), JST PRESTO, the G-COE program of Tokyo Institute of Technology, and a Grant-in-Aid for Scientific Research (S) (No. 22224006) from the Japan Society for the Promotion of Science (JSPS).

REFERENCES

(1) Koshihara, S.; Tokura, Y.; Mitani, T.; Saito, G.; Koda, T. Photoinduced Valence Instability in the Organic Molecular Compound Tetrathiafulvalene-p-Chloranil (TTF-CA). *Phys. Rev. B* **1990**, *42*, 6853−6856.

(2) Iwai, S.; Tanaka, S.; Fujinuma, K.; Kishida, H.; Okamoto, H.; Tokura, Y. Ultrafast Optical Switching from an Ionic to a Neutral State in Tetrathiafulvalene-p-Chloranil (TTF-CA) Observed in Femtosecond Reflection Spectroscopy. *Phys. Rev. Lett.* **2002**, *88*, 057402−1−057402−4.

(3) Kawakami, Y.; Fukatsu, T.; Sakurai, Y.; Unno, H.; Itoh, H.; Iwai, S.; Sasaki, T.; Yamamoto, K.; Yakushi, K.; Yonemitsu, K. Early-Stage Dynamics of Light-Matter Interaction Leading to the Insulator-to-Metal Transition in a Charge Ordered Organic Crystal. *Phys. Rev. Lett.* **2010**, *105*, 246402−1−246402−4.

(4) Uemura, H.; Okamoto, H. Direct Detection of the Ultrafast Response of Charges and Molecules in the Photoinduced Neutral-to-Ionic Transition of the Organic Tetrathiafulvalene-p-Chloranil Solid. *Phys. Rev. Lett.* **2010**, *105*, 258302−1−258302−4.

(5) Wall, S.; Brida, D.; Clark, S. R.; Ehrke, H. P.; Jaksch, D.; Ardavan, A.; Bonora, S.; Uemura, H.; Takahashi, Y.; Hasegawa, T.; et al. A. Quantum interference between charge excitation paths in a solid-state Mott insulator. *Nature Phys.* **2011**, *7*, 114−118.

(6) Fausti, D.; Tobey, R. I.; Dean, N.; Kaiser, S.; Dienst, A.; Hoffmann, M. C.; Pyon, S.; Tkayama, T.; Takagi, H.; Cavalleri, A. Light-Induced Superconductivity in a Stripe-Ordered Cuprate. *Science* **2011**, *331*, 189−191.

(7) Rini, M.; Tobey, R. I.; Dean, N.; Itatani, J.; Tomioka, Y.; Tokura, Y.; Schoenlein, R. W.; Cavalleri, A. Control of the Electronic Phase of a Manganite by Mode-Selective Vibrational Excitation. *Nature* **2007**, *449*, 72−74.

(8) Dienst, A.; Hoffmann, M. C.; Fausti, D.; Petersen, J. C.; Pyon, S.; Takayama, T.; Takagi, H.; Cavalleri, A. Bi-directional Ultrafast Electric-Field Gating of Interlayer Charge Transport in a Cuprate Superconductor. *Nat. Photonics* **2011**, *5*, 485−488.

(9) Pashkin, A.; Kuebler, C.; Ehrke, H.; Lopez, R.; Halabica, A.; Haglund, R. F., Jr.; Huber, R.; Leitenstorfer, A. Ultrafast Insulator-Metal Phase Transition in VO_2 Studied by Multiterahertz Spectroscopy. *Phys. Rev. B* **2011**, *83*, 195120−1−195120−9.

(10) Schmitt, F.; Krchmann, P. S.; Bovensiepen, U.; Moore, R. G.; Rettig, L.; Krenz, M.; Chu, J.-H.; Ru, N.; Perfetti, L.; Lu, D. H.; et al. Transient Electronic Structure and Melting of a Charge Density Wave in $TbTe_3$. *Science* **2008**, *321*, 1649−1652.

(11) Baum, P.; Yang, D.-S.; Zewail, H. 4D Visualization of Transitional Structures in Phase Transformations by Electron Diffraction. *Science* **2007**, *318*, 788−792.

(12) Eichberger, M.; Schaefer, H.; Krumova, M.; Beyer, M.; Demsar, J.; Berger, H.; Moriena, G.; Sciaini, G.; Miller, R. J. D. Snapshots of cooperative atomic motions in the optical suppression of charge density waves. *Nature* **2010**, *468*, 799−802.

(13) Gao, M.; Lu, C.; Jean-Ruel, H.; Liu, L. C.; Marx, A.; Onda, K.; Koshihara, S.; Nakano, Y.; Shao, X. F.; Hiramatsu, T.; et al. Mapping Molecular Motions Leading to Charge Delocalization with Ultrabright Electrons. *Nature* **2013**, *496*, 343−346.

(14) Guerin, L.; Hebert, J.; Cointe, M. B.-L.; Adachi, S.; Koshihara, S.; Cailleau, H.; Collet, E. Capturing One-Dimensional Precursors of a Photoinduced Transformation in a Material. *Phys. Rev. Lett.* **2010**, *105*, 246101−1−246101−4.

(15) Collet, E.; Lemee-Cailleau, M.; Cointe, M.; Cailleau, H.; Wulff, M.; Luty, T.; Koshihara, S.; Meyer, M.; Toupet, L.; Rabiller, P.; Techert, S. Laser-Induced Ferroelectric Structural Order in an Organic Charge-Transfer Crystal. *Science* **2003**, *300*, 612−615.

(16) Matsubara, Y.; Okimoto, Y.; Yoshida, T.; Ishikawa, T.; Koshihara, S.; Onda, K. Photoinduced Neutral-to-Ionic Phase Transition in Tetrathiafulvalene-p-Chloranil Studied by Time-resolved Vibrational Spectroscopy. *J. Phys. Soc. Jpn.* **2011**, *80*, 124711−1−124711−5.

(17) Matsubara, Y.; Yoshida, T.; Ishikawa, T.; Okimoto, Y.; Koshihara, S.; Onda, K. Photoinduced Ionic to Neutral Phase Transition in TTF-CA Studied by Time-resolved Infrared Vibrational Spectroscopy. *Acta Phys. Pol., A* **2012**, *121*, 340−342.

(18) Fukumoto, K.; Fukazawa, N.; Ishikawa, T.; Koshihara, S.; Yamamoto, H. M.; Kato, R.; Onda, K. Photo-induced Structural Changes at a Surface of Organic Single Crystals Observed by Vibrational Sum Frequency Generation Spectroscopy. *Acta Phys. Pol., A* **2012**, *121*, 313−315.

(19) Fukazawa, N.; Shimizu, M.; Ishikawa, T.; Okimoto, Y.; Koshihara, S.; Hiramatsu, T.; Nakano, Y.; Yamochi, H.; Saito, G.; Onda, K. Charge and Structural Dynamics in Photoinduced Phase Transition of $(EDO\text{-}TTF)_2PF_6$ Examined by Picosecond Time-resolved Vibrational Spectroscopy. *J. Phys. Chem. C* **2012**, *116*, 5892−5899.

(20) Suemoto, T.; Fukaya, R.; Asahara, A.; Nakajima, M.; Tokoro, H.; Ohkoshi, S. Dynamics of Photoinduced Phase Transitions in Hexacyanoferrate Studied by Infrared and Raman Spectroscopy. *Phys. Status Solidi B* **2011**, *248*, 477−481.

(21) Asahara, A.; Nakajima, M.; Fukaya, R.; Tokoro, H.; Ohkoshi, S.; Suemoto, T. Photo-Induced Phase Switching Dynamics in $RbMn[Fe(CN)_6]$ Probed by Accumulation Free Mid-Infrared Spectroscopy. *Phys. Status Solidi B* **2011**, *248*, 491−494.

(22) Ishikawa, T.; Onda, K.; Koshihara, S. Photo-Induced Phase Transition in Strongly Electron−Lattice and Electron-Electron Correlated Molecular Crystals. *Crystals* **2012**, *2*, 1067−1083.

(23) Special Topics on Organic Conductors; Kagoshima, S.; Kanoda, K.; Mori, T., Eds.; *J. Phys. Soc. Jpn.* **2006**, *75*, 051001−051016.
(24) Topical Review on Focus on Organic Conductors ; Uji, S.; Mori, T.; Takahashi, T., Eds.; *Sci. Technol. Adv. Mater.* **2009**, *10*, 020301−024314.
(25) Dressel, M. Ordering Phenomena in Quasi-One-Dimensional Organic Conductors. *Naturswissenschaften* **2007**, *94*, 527−541.
(26) Miyagawa, K.; Kanoda, K.; Kawamoto, A. NMR Studies on Two-Dimensional Molecular Conductors and Superconductors: Mott Transition in κ-(BEDT-TTF)$_2$X. *Chem. Rev.* **2004**, *104*, 5635−5654.
(27) Kato, R. Conducting Metal Dithiolene Complexes: Structural and Electronic Properties. *Chem. Rev.* **2004**, *104*, 5319−5346.
(28) Kanoda, K.; Kato, R. Mott Physics in Organic Conductors with Triangular Lattices. *Annu. Rev. Condens. Matter. Phys.* **2011**, *2*, 167−188.
(29) Special Issue on Photo-Induced Phase Transitions and Their Dynamics; Gonokami, M.; Koshihara, S., Eds.; *J. Phys. Soc. Jpn.* **2006**, *75*, 011001−011008.
(30) Nasu, K. *Photo Induced Phase Transition*; World Scientific: Singapore, 2003.
(31) Dressel, M.; Drichko, N. Optical Properties of Two-Dimensional Organic Conductors: Signatures of Charge Ordering and Correlation Effects. *Chem. Rev.* **2004**, *104*, 5689−5716.
(32) Drozdova, O.; Yakushi, K.; Yamamoto, K.; Ota, A.; Yamochi, H.; Saito, G.; Tashiro, H.; Tanner, B. D. Optical Characterization of 2kF Bond-Charge-Density Wave in Quasi-One-Dimensional 3/4-filled (EDO-TTF)$_2$X (X=PF_6 and AsF_6). *Phys. Rev. B* **2004**, *70*, 075107−1−075107−8.
(33) Yakushi, K.; Yamamoto, K.; Swietlik, R.; Wojciechowski, R.; Suzuki, K.; Kawamoto, T.; Mori, T.; Misaki, Y.; Tanaka, K. Spectroscopic Studies of Charge-Ordering System in Organic Conductors. *Macromol. Symp.* **2004**, *212*, 159−168.
(34) Yamamoto, T.; Uruichi, M.; Yamamoto, K.; Yakushi, K.; Kawamoto, A.; Taniguchi, H. Examination of the Charge-Sensitive Vibrational Modes in Bis(ethylenedithio)tetrathiafulvalene. *J. Phys. Chem. B* **2005**, *109*, 15226−15235.
(35) Yamamoto, K.; Yamamoto, T.; Yakushi, K.; Pecile, C.; Meneghetti, M. Bond and Charge-Density Waves in (DI-DCNQI)$_2$Ag (DI-DCNQI=2,5-Diiodo-N,N′-Dicyanoquinediimine) Studied by Single-Crystal Infrared and Raman Spectroscopy. *Phys. Rev. B* **2005**, *71*, 045118−1−045118−10.
(36) Tanaka, M.; Yamamoto, K.; Uruichi, M.; Yamamoto, T.; Yakushi, K.; Kimura, S.; Mori, H. Infrared and Raman Study of the Charge-Ordered State in the Vicinity of the Superconducting State in the Organic Conductor β-(meso-DMBEDT-TTF)$_2PF_6$. *J. Phys. Soc. Jpn.* **2008**, *77*, 024714−1−024714−8.
(37) Yamamoto, T.; Yamamoto, H. M.; Kato, R.; Uruichi, M.; Yakushi, K.; Akutsu, H.; Sato-Akutsu, A.; Kawamoto, A.; Turner, S. S.; Day, P. Inhomogeneous Site Charges at the Boundary between the Insulating, Superconducting, and Metallic phases of β″-type Bis-Ethylenedithio-Tetrathiafulvalene Molecular Charge-Transfer Salts. *Phys. Rev. B* **2008**, *77*, 205120−1−205120−14.
(38) Yue, Y.; Yamamoto, K.; Uruichi, M.; Nakano, C.; Yakushi, K.; Yamada, S.; Hiejima, T.; Kawamoto, A. Nonuniform Site-Charge Distribution and Fluctuations of Charge Order in the Metallic State of α-(BEDT-TTF)$_2I_3$. *Phys. Rev. B* **2010**, *82*, 075134−1−075134−8.
(39) Yamamoto, T.; Nakazawa, Y.; Tamura, M.; Fukunaga, T.; Kato, R.; Yakushi, K. Vibrational Spectra of [Pd(dmit)$_2$] Dimer (dmit = 1,3-dithiole-2-thione-4,5-dithiolate): Methodology for Examining Charge, Inter-Molecular Interactions, and Orbital. *J. Phys. Soc. Jpn.* **2011**, *80*, 074717−1−074717−16.
(40) Yamamoto, K.; Kowalska, A. A.; Yue, Y.; Yakushi, K. Vibronic Activation of Molecular Vibrational Overtones in the Infrared Spectra of Charge-Ordered Organic Conductors. *Phys. Rev. B* **2011**, *84*, 064306−1−064306−13.
(41) Tamura, M.; Kato, R. Variety of Valence Bond States Formed of Frustrated Spins on Triangular Lattices Based on a Two-Level System Pd(dmit)$_2$. *Sci. Technol. Adv. Mater.* **2009**, *10*, 024304−1−024304−12.
(42) Yamashita, M.; Nakata, N.; Senshu, Y.; Nagata, M.; Yamamoto, H. M.; Kato, R.; Shibauchi, T.; Matsuda, Y. Highly Mobile Gapless Excitations in a Two-Dimensional Candidate Quantum Spin Liquid. *Science* **2010**, *328*, 1246−1248.
(43) Itou, T.; Oyamada, A.; Maegawa, S.; Kato, R. Instability of a Quantum Spin Liquid in an Organic Triangular-Lattice Antiferromagnet. *Nat. Phys.* **2010**, *6*, 673−676.
(44) Nakao, A.; Kato, R. Structural Study of Low Temperature Charge-Separated Phases of Pd(dmit)2-Based Molecular Conductors. *J. Phys. Soc. Jpn.* **2005**, *74*, 2754−2763.
(45) Tamura, M.; Nakao, A.; Kato, R. Frustration-Induced Valence-Bond Ordering in a New Quantum Triangular Antiferromagnet Based on [Pd(dmit)$_2$]. *J. Phys. Soc. Jpn.* **2006**, *75*, 093701−1−093701−4.
(46) Shimizu, Y.; Akimoto, H.; Tsujii, H.; Tajima, A.; Kato, R. Mott Transition in a Valence-Bond Solid Insulator with a Triangular Lattice. *Phys. Rev. Lett.* **2007**, *99*, 256403−1−256403−4.
(47) Underhill, A. E.; Clark, R. A.; Marsden, I.; Allan, M.; Friend, R. H.; Tajima, H.; Naito, T.; Tamura, M.; Kuroda, H.; Kobayashi, A.; et al. Structural and Electronic Properties of Cs(Pd(dmit)$_2$)$_2$. *J. Phys.: Condens. Matter* **1991**, *3*, 933−954.
(48) Tamura, M.; Kato, R. Valence Instability in a Dimer of Two-Orbital System: Possible Charge Separation due to 'Negative U' Effect. *Chem. Phys. Lett.* **2004**, *387*, 448−452.
(49) Tamura, M.; Takenaka, K.; Takagi, H.; Sugai, S.; Tajima, A.; Kato, R. Spectroscopic Evidence for the Low-Temperature Charge-Separated State of [Pd(dmit)$_2$] Salts. *Chem. Phys. Lett.* **2005**, *411*, 133−137.
(50) Tamura, M.; Tajima, A.; Kato, R. Novel Phase Transition in Et_2Me_2Sb[Pd(dmit)$_2$]$_2$ at 70 K: A Possible Mechanism Based on Strong Dimerization of Two-Level Molecules. *Synth. Met.* **2005**, *152*, 397−400.
(51) Ishikawa, T.; Fukazawa, N.; Matsubara, Y.; Nakajima, R.; Onda, K.; Okimoto, Y.; Koshihara, S.; Lorenc, M.; Collet, E.; Tamura, M.; Kato, R. Large and Ultrafast Photoinduced Reflectivity Change in the Charge Separated Phase of Et_2Me_2Sb[Pd(1,3-dithiol-2-thione-4,5-dithiolate)$_2$]$_2$. *Phys. Rev. B* **2009**, *80*, 115108−1−115108−8.
(52) Canadell, E.; Ravy, S.; Pouget, J. P.; Brossard, L. Concerning the Band Structure of D(M(dmit)$_2$)$_2$ (D=TTF,Cs,NMe_4); M=Ni,Pd) Molecular Conductors and Superconductors: Role of the M(dmit)2 Homo and Lumo. *Solid State Commun.* **1990**, *75*, 633−638.
(53) Ishikawa, T.; Tanaka, T.; Fukazawa, N.; Matsubara, Y.; Onda, K.; Okimoto, Y.; Koshihara, S.; Tamura, M.; Kato, R.; in preparation for publication.
(54) Aonuma, S.; Sawa, H.; Kato, R. Preparation, Structure and Conductivity of Et_2Me_2Z (Z=P,As,Sb) Salts of M(dmit)$_2$ and M(dmise)$_2$ (M=Ni,Pd). *Synth. Met.* **1997**, *86*, 1881−1882.
(55) Note that the IR active A mode due to the tetramerization is sensitive to interdimer interaction. However, the intensity of the IR active A mode is often small. In our time-dependent spectra, such vibrational modes cannot be observed.
(56) As described in ref 39, the C band in the low-temperature phase is split into four factor groups. The number of C mode is four. The broad line shape is ascribed to not only the e-mv interaction but also the overlapping between several C bands.
(57) Strictly speaking, the two dips of the D mode originate from different dimer. The dip at 1263 and 1302 cm^{-1} are assigned to the neutral and divalent dimers, respectively.[39]
(58) Okamoto, H.; Ishige, Y.; Tanaka, S.; Kishida, H.; Iwai, S.; Tokura, Y. Photoinduced Phase Transition in Tetrathiafulvalene-p-Chloranil Observed in Femtosecond Reflection Spectroscopy. *Phys. Rev. B* **2004**, *70*, 165202−1−165202−18.
(59) Okamoto, H.; Matsuzaki, H.; Wakabayashi, T.; Takahashi, Y.; Hasegawa, T. Photoinduced Metallic State Mediated by Spin-Charge Separation in a One-Dimensional Organic Mott Insulator. *Phys. Rev. Lett.* **2007**, *98*, 037401−1−037401−4.
(60) Okimoto, Y.; Matsuzaki, H.; Tomioka, Y.; Kezsmarki, I.; Ogasawara, T.; Matsubara, M.; Okamoto, H.; Tokuya, Y. Ultrafast Photoinduced Formation of Metallic State in a Perovskite-Type

Manganite with Short Range Charge and Orbital Order. *J. Phys. Soc. Jpn.* **2007**, *76*, 043702−1−043702−4.
(61) Okimoto, Y.; Peng, X.; Tamura, M.; Morita, T.; Onda, K.; Ishikawa, T.; Koshihara, S.; Todoroki, N.; Kyomen, T.; Itoh, M. Ultrasonic Propagation of a Metallic Domain in $Pr_{0.5}Ca_{0.5}CoO_3$ Undergoing a Photoinduced Insulator-Metal Transition. *Phys. Rev. Lett.* **2009**, *103*, 027402−1−027402−4.
(62) Tanimura, K. Femtosecond Time-Resolved Reflection Spectroscopy of Photoinduced Ionic-Neutral Phase Transition in TTF-CA Crystals. *Phys. Rev. B* **2004**, *70*, 144112−1−144112−11.